doi.org/10.52568/001705/JCSP/47.03.2025

Characterization of the Pharmacological Mechanism and Protein Binding Mechanism of Rhaponticin: Network Pharmacology Combined with Multispectral Analysis Insight

[1]A'ning Xu, [2]Yanan Wu, [2]Ming Guo*, [1]Keli Zhao, [3]Yubo Zhang, and [3]Xiangjun Dong
[1]*College of Environment and Resources, Zhejiang Agriculture & Forestry University, Hangzhou, Zhejiang, 311300, China.*
[2]*College of Chemistry and Materials, Zhejiang Agriculture & Forestry University, Hangzhou, Zhejiang, 311300, China.*
[3]*School of Public Health and Health Sciences, Tianjin University of Traditional Chinese Medicine.*
guoming@zafu.edu.cn*

(Received on 28th September 2023, accepted in revised form 3rd May 2025)

Summary: This paper explores the molecular mechanism of the interaction of rhodopsin (RT), an active ingredient of traditional Chinese medicine, with bovine lactoferrin (BLF) and its potential role in cancer therapy. The protein action network of RT on tumors was explored by network pharmacology; multispectral and molecular simulation techniques were used to study the interaction mechanism between RT and BLF, and the mediating role of metal ions with the RT-BLF system. The network pharmacology results showed that RT-BLF had similar binding energies to RT-validated core target proteins, confirming BLF as a potential target of RT for cancer treatment. It was further verified by multispectral analysis that the binding of RT-BLF formed spontaneous and stable complexes and the burst mechanism was dominated by static quenching, and the metal ions Co (II) and Ni (II) acted as bridges in the reaction to enhance the interaction between RT-BLF. The molecular modeling results showed that hydrogen and hydrophobic bonds play important roles in the RT-BLF system to form stable complexes. This study elucidated the mechanism of interaction between RT and BLF, and verified the bridging role of metal ions in the RT-BLF system to promote stable binding, which provides a basis for the application of RT and a new idea for the study of active ingredients in traditional Chinese medicine.

Key words: Turmeric glycoside; Lactoferrin; Network pharmacology; Multi spectral; Molecular modeling.

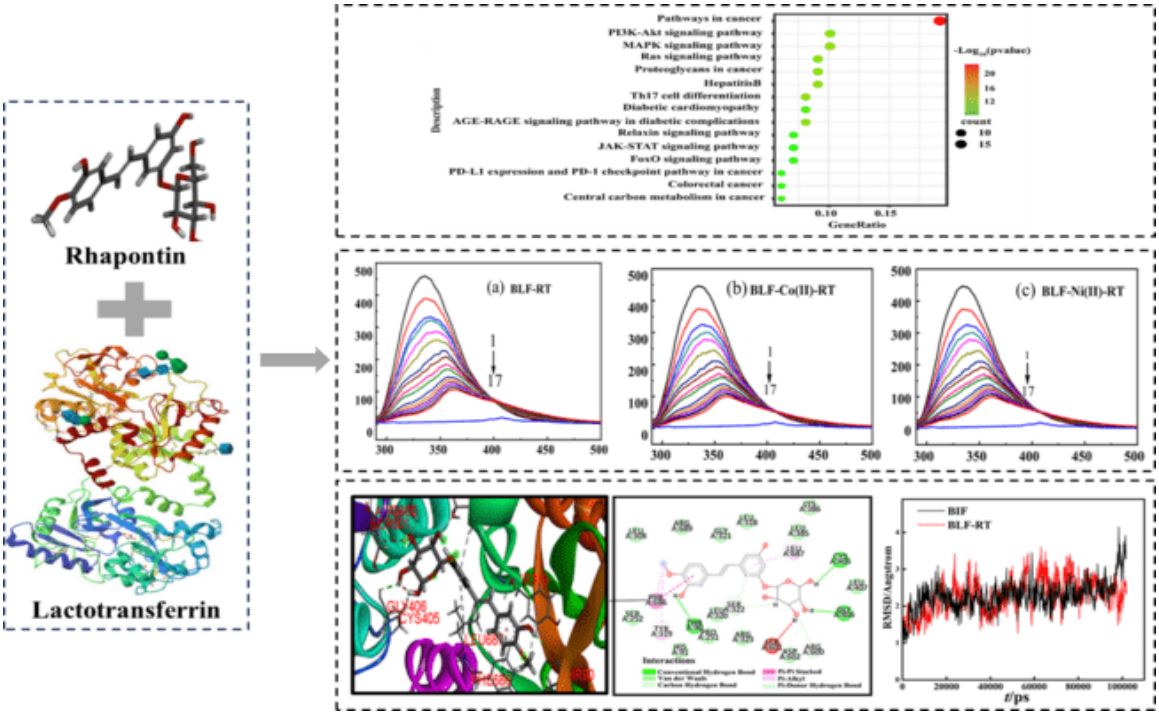

Using network pharmacology to analyse the detailed molecular mechanisms and therapeutic targets of RT in cancer disease regulation. Molecular docking and spectroscopy have revealed the molecular mechanism of binding between RT and BLF, providing useful clues for studying the binding mechanism between pharmacologically active RT and functional proteins.

*To whom all correspondence should be addressed.

Introduction

Bovine lactoferrin (BLF) is a globulin derived from the composition of bovine whey. Structurally, it consists of approximately 700 members and amino acid residues with a molecular weight of approximately 80 kDa [1]. It has been reported that lactoferrin is not only involved in iron transport but also has many important biological functions such as broad-spectrum antibacterial, antioxidant, anticancer and immune system regulation[2-5]. It is therefore considered a promising anticancer drug ligand, transport medium and food additive. By studying the combination of drugs and BLF under physiological conditions, pharmacodynamic information can be obtained.

Rhodopsin (RT) is a styrene derivative rich in huangjing. (Fig 1) In addition to its anticancer activity and amelioration of retinal oxidative stress and inflammation [6,7], it also has rich pharmacological activities, including anti-tumour, antithrombotic and antioxidant effects [8,9]. Studying the binding reaction of RT using BLF as a template can provide a deeper understanding of the mechanism of action between RT and BLF, thereby elucidating the pharmacological effects of RT and providing a reference for its new drug development and clinical application.

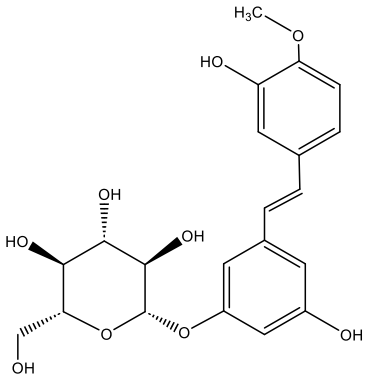

Fig 1: The chemical structure of Rhodopsin.

Metal ions play an important role in many life activities; cobalt has been found to be an important component of haemoglobin and vitamin B_{12}, and deficiency of cobalt in organisms leads to anaemia [10]; nickel ions can be efficiently chelated by serum albumin and transported to various parts of the body, and other substances such as L-histidine and megaglobulin can also be bound to nickel ions [11]. In addition, BLF as a template protein can bind to metal ions (iron) and it is necessary to investigate the effects of other metal ions on BLF. The combination of spectral experiments and network pharmacology brings together a number of advantages such as ease of use, high sensitivity, good selectivity, low sample consumption and great cost savings [12-14].

In this study, to enrich the medicinal scope of RT, we used network pharmacology to obtain the core targets of RT and its associated cancers using BLF as a template, performed enrichment analysis to obtain the signalling pathways for the treatment of the associated cancers, and applied molecular docking to compare the binding energies of RT with BLF and the core targets. Since target proteins are difficult to obtain, BLF, which has a similar binding energy to the core target, was selected for subsequent experiments. Meanwhile, BLF as a template protein can bind to metal ions and it is necessary to investigate the effects of other metal ions on BLF. The interactions of RT with BLF mediated by Co (II) and Ni (II) ions were verified at the molecular level by multispectroscopy, which in turn corresponded to the pharmacodynamic basis of RT binding to BLF-associated cancer target proteins. Molecular docking and kinetic simulations were used to elucidate the intermolecular forces and conformational relationship.

Experimental

Materials and Instruments

Experimental materials: Rhaponticin (RT, ≥99%, Nanjing Zelang Bio-medic Technologies Inc., Ltd, China); Bovine lactoferrin (BLF, ≥98%, Wako Pure Chemical Industries, Ltd; Art. No.: KWM6492, Japan); Trihydroxymethy laminomethane (Tris, GR) were purchased from Shanghai Huamei Biology Engineer Company; HCl, Co $(NO_3)_2$, Ni $(NO_3)_2$ and NaCl were of analytical grade and were used without further purification. The 0.1 mol·L^{-1} Tris-HCl buffer of pH=7.4 (0.10 mol·L^{-1} NaCl was used to keep the ionic strength constant) was prepared. Double-distilled water was used throughout.

Experimental instruments: All fluorescence spectra were recorded on an F-4500 spectrophotometer (Hitachi, Japan) equipped with a xenon lamp and 1.0 cm quartz cells, using 2.5nm/2.5nm slit widths. The UV-absorption spectra were performed on a UV-2450 ultraviolet-visible spectrophotometer (Shimadzu, Japan) equipped with 1.0 cm cuvette. All pH values were measured on a ZD-2 digital pH-meter (Shanghai Lei Ci Device Works, Shanghai, China) with a combined glass electrode.

Network pharmacology

Database Platform and Software

Database and software information used in the experiment is listed as Table-1.

Table-1: Database and software information used in the experiment.

Database platform	Website
TCMSP	https://tcmsp-e.com/tcmsp.php
Pharm Mapper	http://lilab-ecust.cn/pharmmapper/index.html
Uniprot	https://www.uniprot.org/
Gene Cards	https://www.genecards.org/
Venny	https://bioinfogp.cnb.csic.es/tools/venny/
STRING	https://cn.string-db.org/
Metascape	http://metascape.org/gp/index.html
PDB	https://www.rcsb.org/

Acquisition of RT components and potential targets

In the TCMSP database [15] , search with the keyword "RHAPONTIN", download small molecule "mol2" format and upload it to the Pharm Mapper database [16] for target prediction. The prediction type is "Human Protein Targets Only (v2010, 2241)". Copy the Uniprot ID corresponding to the predicted target to the Retrieve/ID mapping interface of the Uniprot database [17] and convert it to Gene Name format. The reverse pharm acophore matching method is used to search for "BLF" through Gene Cards to obtain related diseases. Then, the Gene Cards database [18] is used to search for target proteins of the diseases, and they are summarized and screened. In order to further understand the protein level interaction mechanism between the targets of turmeric glycoside and lactoferrin related diseases, Venny [19] was used to create Venn diagrams to obtain the intersection targets of turmeric glycoside and diseases.

Network construction of intersection target proteins

Use STRING [20] to construct a network of intersecting target proteins, obtain target information, and use the CytoScape 3.8.2 software Analyze Network plugin to calculate the degree value. After analysis, visualize the analysis based on the size of the degree.

Molecular docking verification

Evaluate the strength of the protein relationship in the PPI network based on the magnitude of the Indegree value, and select the top 5 target proteins for molecular docking with turmeric glycoside using Auto Dock software.

Enrichment analysis of GO and KEGG pathways

Input 41 core targets into the Metascape database [21] platform and screen based on the following conditions: $P<0.01$, minimum overlap value of 3, and minimum enrichment of 1.5. Select GO molecular functions, GO biological processes, GO cell components, and KEGG pathways for enrichment analysis to obtain the main signaling pathways related to gene targets. Using and enriching the top 10 clusters through log*p* and the number of enriched genes, using Original 2021 for visual analysis.

RT- Disease- Network Pathway Map

In order to more intuitively demonstrate the role of the core target of emodin in the treatment of diseases, this article uses CytoScape software to construct a network diagram of emodin related disease target pathways.

Spectrometric Determination of the Interaction between RT and BLF Molecules

BLF and RT, RT-Co (II), RT-Ni (II) (the molar ratio=1:1) were dissolved in Tris-HCl buffer. The concentrations of BLF was 1.00×10^{-5} mol·L^{-1}, and RT, RT-Co (II) (the molar ratio=1:1) and RT-Ni (II) (the molar ratio=1:1) were 1.00×10^{-3} mol·L^{-1}, respectively.

2.5 mL BLF (1.00×10^{-5} mol·L^{-1}) was added to the quartz cell, and the range of the RT (1.00×10^{-3} mol·L^{-1}) solution was gradually added into the cell using a micro-injector (the total accumulated volume< 200 μL), stirring time was enough kept to show the fluorescence spectra non-time-dependent change after mixing the solutions. The fluorescence quenching spectra were measured at excitation wavelength 282 *nm*, and the excitation and emission widths (each 2.5*nm*) and scan speed (1200 *nm*/min) were constantly maintained throughout the measurement (Tris-HCl buffer was used to adjust zero). The synchronous fluorescence spectra of BLF-RT solution system was recorded by simultaneously scanning the excitation and emission monochromators with the wavelength intervals $\Delta\lambda$=60 *nm* and $\Delta\lambda$=15 *nm* respectively. The range of synchronous scanning was 230-310 *nm* ($\Delta\lambda$=60 *nm*) and 270-320 *nm* ($\Delta\lambda$=15 *nm*), separately.

The sample of RT (1.0×10^{-5} mol·L^{-1}) was brought to 1.00 cm cuvette *versus* a blank of buffer, and the UV-absorption spectra of RT was measured by the UV-2450 ultraviolet-visible spectrophotometer and a spectral scanning curve was made.

Inner filter effect of the quencher was corrected:

$$F_e = F_m e^{(A_1+A_2)/2} \quad (1)$$

where F_e and F_m are the corrected and measured fluorescence, respectively; A_1 and A_2 are the sum of proteins and ligands at the excitation and max emission wavelengths, respectively.

In order to study the effect of metal ions, the fluorescence quenching spectra and synchronous fluorescence spectra of BLF-RT-Co (II) and BLF-Ni (II) -RT solution system, and the UV-absorption spectra of RT-M^{2+} (M^{2+}=Co^{2+}, Ni^{2+}; 1.0×10^{-5} mol·L^{-1}) solution system were measured according the same method as above.

Physical Modeling of Interactions between RT and BLF Molecules

Molecular docking

Obtain the "BLF" lactoferrin crystal structure "pdb" file from the PDB database [22]. Open the Discovery Studio software to remove water, add hydrogen, calculate charge, and save the file as a "pdbqt" file. Use Chemdraw to construct RT small molecule ligands, optimize energy, and also save them as "pdb" files. AutoDock software adds hydrogen and charge to it, and also saves it as an open "pdbqt" file. Open the "pdbqt" format of lactoferrin using AutoDock, set the grid diagram in the Grid module, wrap the protein and small molecules together, and save the output in "gpf" format. The Docking of AutoDock opens the "pdbqt" files of BLF and RT, uses the Lamarchian genetic algorithm (LGA) method for conformational search, and saves the output in "dpf" format, Perform the same operation on RT.

Molecular dynamic simulation

Use YASARA software to locate the "pdb" files of BLF and RT to the active site of BLF, so that small molecules can approach the active site. Conduct structural analysis, set the environmental pH to 7.4, and then optimize the system energy. After optimizing the system, save the "YASARA" scene file, and then specify a kinetic script to run to 100ns. Perform RMSF value analysis first, and then specify a script for RMSD analysis. Use Origin2021 software for graphic analysis.

Experimental Results and Discussion

Research on the Mechanism of RT Action Based on Network Pharmacology

Target points for RT treatment of diseases

Through Pharma Mapper, 299 RT-related targets were obtained. 74 targets were screened based on the condition that disease does not equal NONE. Obtain 5 diseases related to BLF through gene card search, and then search for target proteins related to this disease. Then, using Score>10 as the screening condition, 1552 target proteins were obtained, and 41 intersecting targets were selected to draw Venn plots. These targets are considered potential targets for the treatment of diseases with turmeric glycosides, as shown in Fig 2.

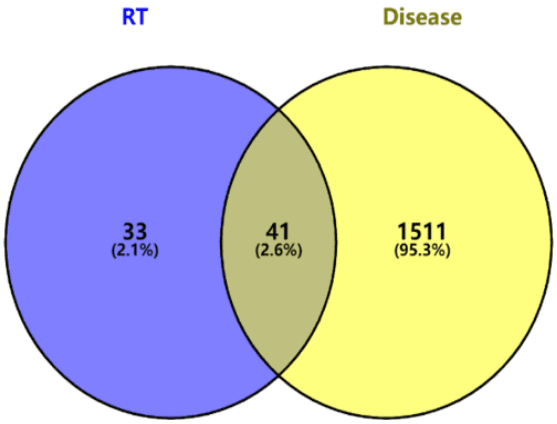

Fig. 2: Venn diagram of RT target-BLF related disease target.

Construction of Intersection Target Protein Interaction Network

Fig 3 is a protein interaction network sorted based on the size of the Index value. The index value reflects the relationships between proteins. The higher the index value, the more target proteins interact with the target protein and the more important the target protein is in the network. As shown in the Fig 3, the top 5 Degree values are ALB, EGFR, MMP9, HRAS and CASP3.

Molecular docking verification

Molecular docking of five target proteins with BLF using AutoDock. The binding energy of the target protein is below zero, indicating its spontaneous binding to RT. The free binding energies of ALB, EGFR, MMP9, HRAS, CASP3

and BLF are all less than -5.0 kcal/mol, indicating their strong binding ability and stable conformation. The binding ability of BLF to five target proteins is similar, which means that emodin and lactoferrin can be targeted drugs for disease treatment. The results of optimum free binding energy of protein to RT molecule is shown in Table-2.

Table-2: Optimum free binding energy of protein to RT molecule.

Protein	PDB ID	Resolution	Binding Energy
ALB	4BKE	2.35 Å	-8.90kcal/mol
EGFR	5WB7	2.94 Å	-8.07kcal/mol
MMP9	5TH6	1.70 Å	-8.27kcal/mol
HRAS	6Q21	1.95 Å	-8.58kcal/mol
CASP3	5I9B	1.80 Å	-8.08kcal/mol
BLF	1BLF	2.80 Å	-8.10kcal/mol

GO analysis and KEGG pathway enrichment analysis

The enrichment analysis of the core targets identified a total of 494 biological processes, 51 molecular functions, 43 cellular components (as shown in Fig 4 a) and 99 signalling pathways (as shown in Fig 4b).

Fig 4 (a) shows the results of the Gene Ontology analysis, with multiple targets enriched in each pathway. The biological processes mainly involved in BIF (GO-BP) include hormone response, reactive oxygen species response, protein phosphorylation in cell localisation regulation, protein phosphorylation regulation, negative regulation of external apoptosis signals/cell proliferation, response to xenobiotic stimuli, and growth regulation. Molecular functions (GO-MF) are mainly protein kinase activity and nuclear receptor activity. The most important cellular components (GO-CC) are membrane rafts, cytoplasmic perinuclear regions, vesicle regions, etc.

Fig 5 (b) shows the RT-target pathway network constructed in CytoScape 3.8.2, which indicates that among the targets associated with RT and signalling pathways, target genes such as cancer pathway, P13-Akt information pathway in cancer protein polysaccharide cluster, MAPK signalling pathway, PD-LI expression, PD-1 checkpoint pathway in tumours and Th17 account for a large proportion in the network targets. Therefore, from the above conclusion, it can be concluded that the reason why RT plays a role in regulating cancer may be due to its target gene is also the core gene of the cancer signalling pathway.

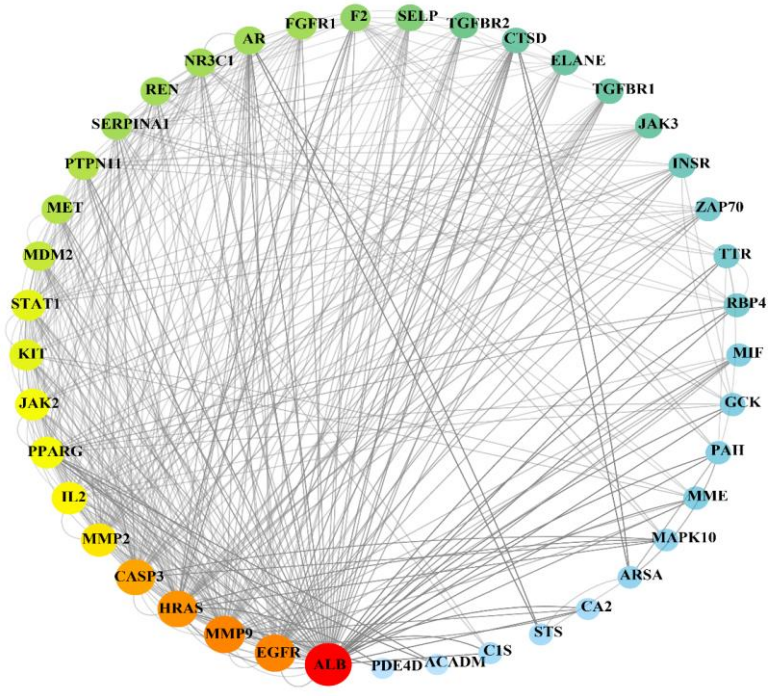

Fig. 3: Network construction of intersection target protein.

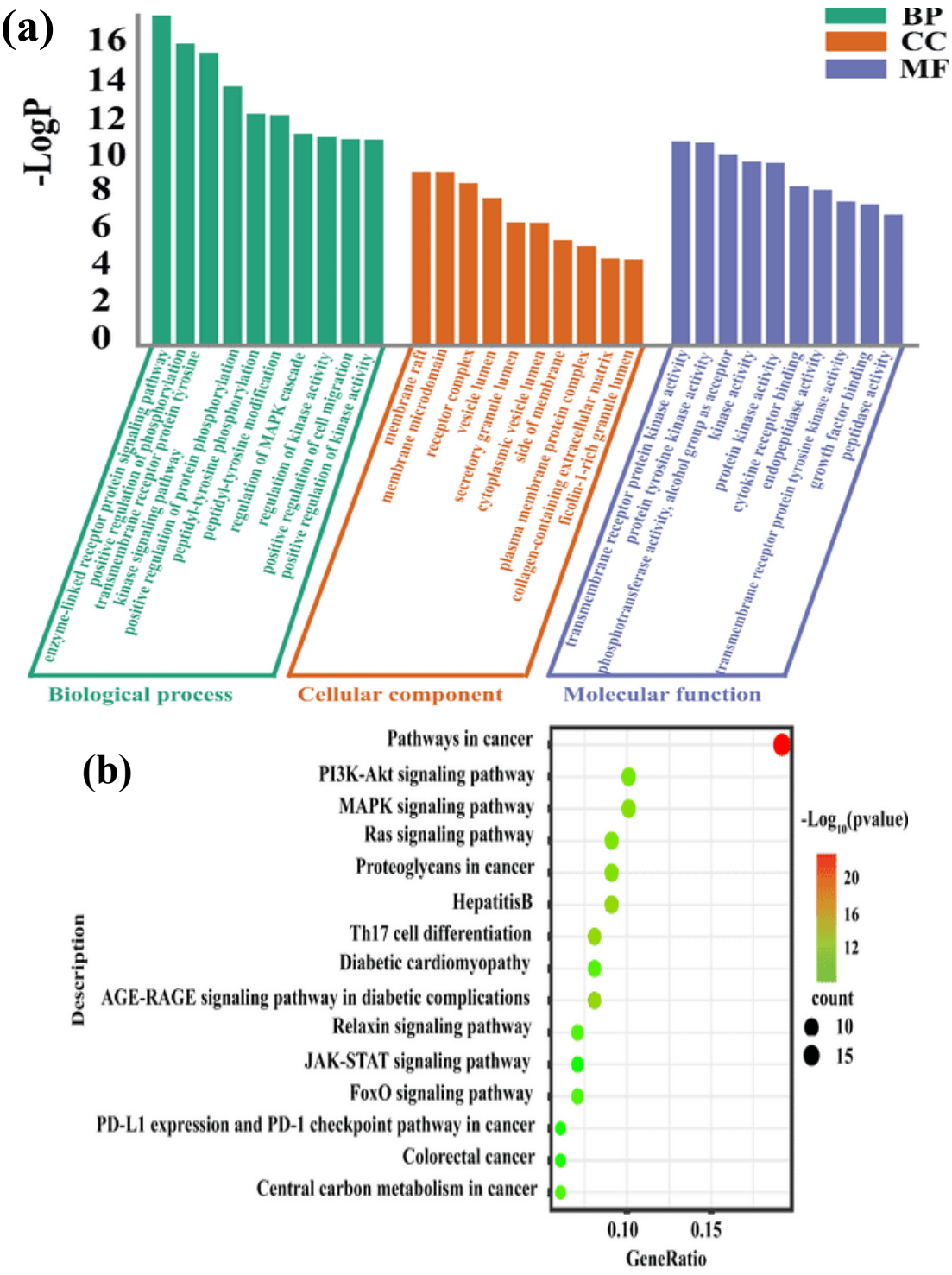

Fig 4: The enrichment analysis of RT core targets.
(a) GO-BP enrichment analysis, GO-CC enrichment analysis, GO-MF enrichment analysis; (b) KEGG Pathway enrichment analysis.

RT -Disease -Pathway Network Diagram

A network of "RT disease core target pathways" was constructed, generating 39 nodes and 147 edges. The size of the target gene node is related to the number of connections, indicating a strong relationship between the target and gene nodes. The most tightly connected target in the whole network is HRAS; the pathway is Pathwas in cancer.

The fluorescence spectra and interaction mechanism of RT/RT-Co (II) /RT-Ni (II) binding with BLF

Fluorescence spectra of RT, RT Co (II), and RT Ni (II) binding reactions with BLF

Fig 6 shows the fluorescence emission spectra of BLF at certain concentration, and the regular quenching spectra by various concentrations of RT/RT-M^{2+} (M^{2+}=Co^{2+}, Ni^{2+}).

From Fig 6, it can be seen that as the concentration of RT/RT-M^{2+} in the reaction system increases, the fluorescence of BLF is regularly quenched, and the maximum emission peak positions of the fluorescence in the interaction between RT/RT-M^{2+} and BLF all undergo a significant red shift (28 nm), suggesting that RT/RT-M^{2+} significantly alters the chemical environment in some micro-regions of the BLF molecular structure, and overall reduces the hydrophobicity in the vicinity of the drug molecule binding sites; the major fluorescent chromophores originally encapsulated in the BLF macromolecules are generally more exposed to polar solvents [23]. Meanwhile, the maximum fluorescence emission peak positions of metal ions Co (II) and Ni (II) on BLF molecules did not change, indicating that in the RT-M^{2+}-BLF mixed solution system, although M^{2+} ions mediate the binding reaction of RT-BLF, the main result is still the RT molecule that plays a major role in the RT-M^{2+} and BLF system.

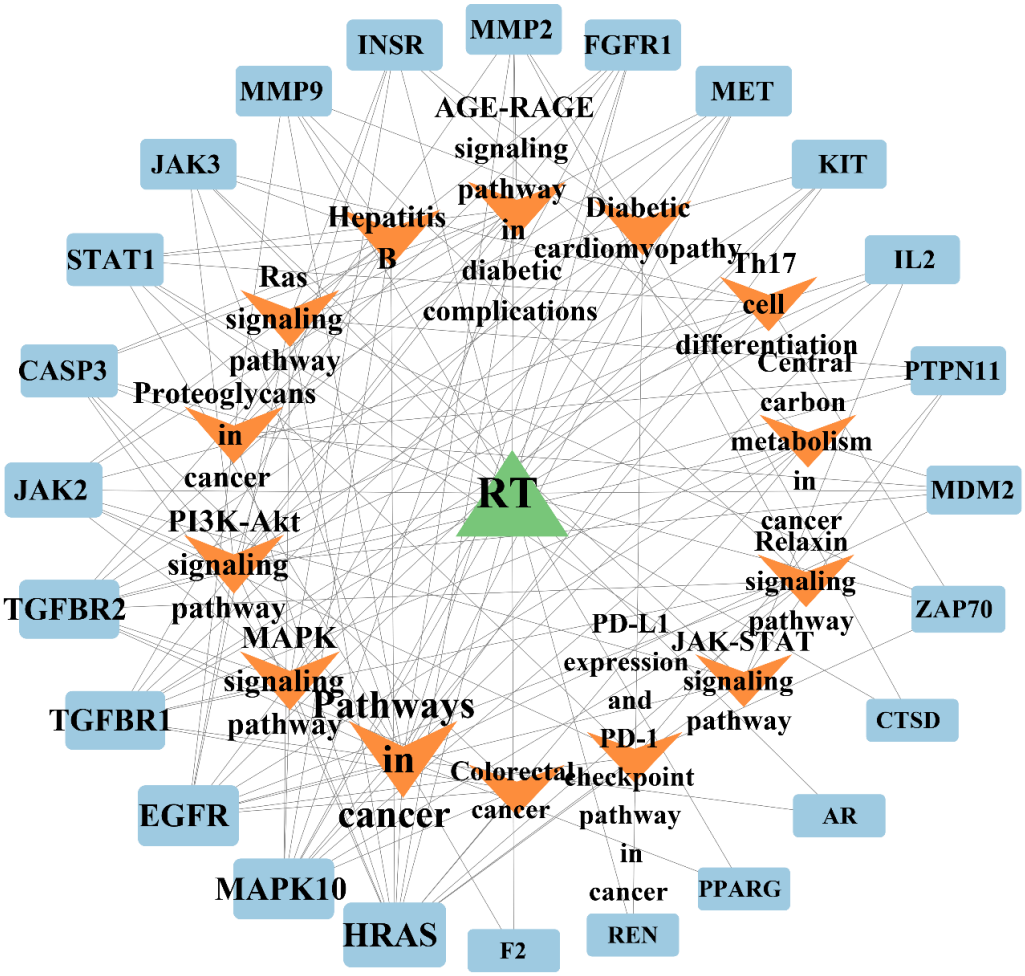

Fig. 5: RT core disease target -pathway network.

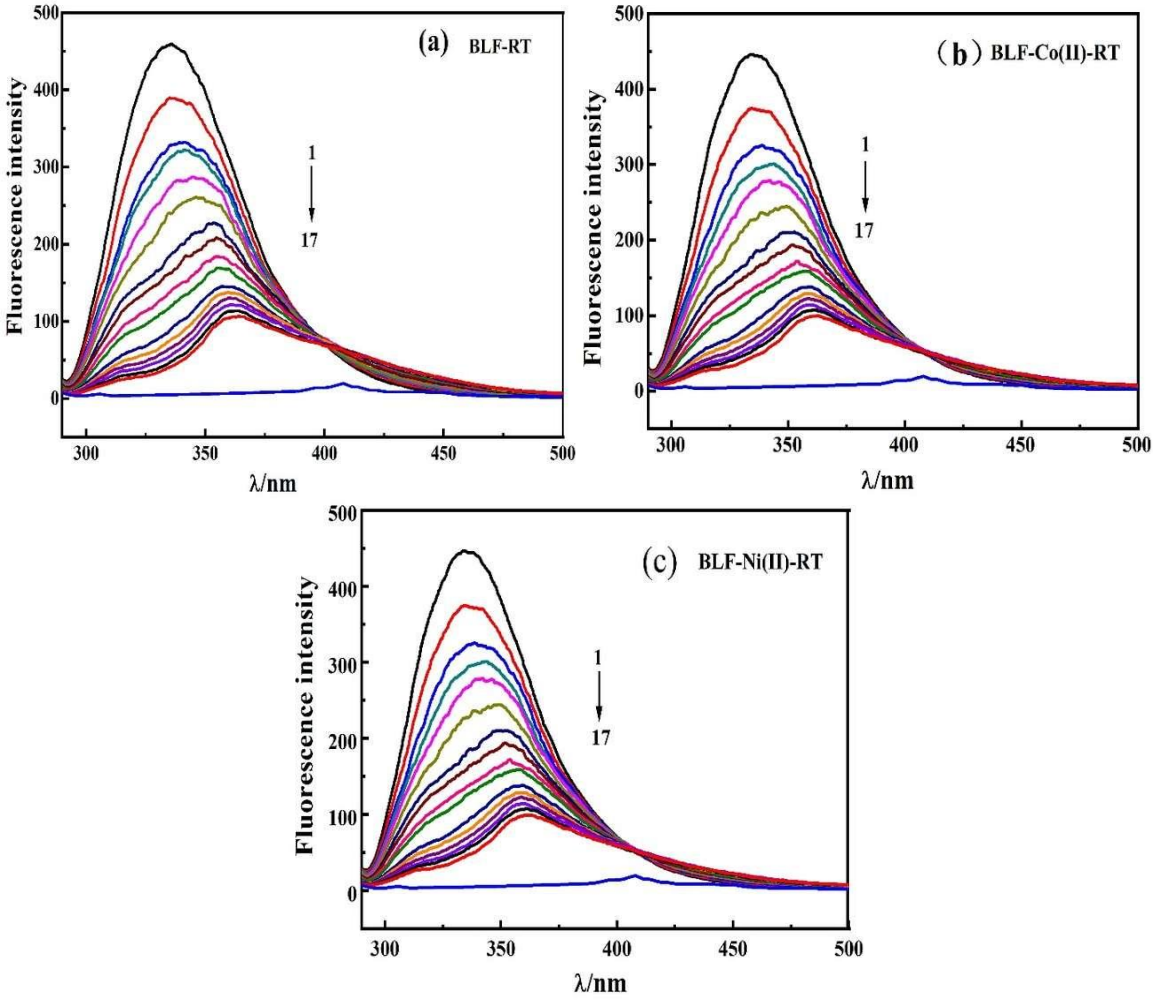

Fig. 6: Intensity of RT (a), RT-Co (II) (b) and RT-Ni (II) (c) on the quenching of BLF fluorescence. Conditions: pH=7.40, λ_{ex}=282*nm*,c_{BLF}=1.0×10^{-5}mol·L^{-1},c_{RT}/$c_{RT\text{-}Co\ (II)}$ /$c_{RT\text{-}Ni\ (II)}$ (×10^{-5}mol·L^{-1}), 1 to 16: 0, 0.40, 0.80, 1.00, 1.20, 1.60, 2.04, 2.48, 2.88, 3.32, 4.20, 4.60, 5.04, 5.48, 5.92, 6.36.The line of 17 is the fluorescence of RT. [The up-right diagram is the fluorescence quenching of BLF in the presence of Co (II) and Ni (II)].

The fluorescence quenching process usually includes dynamic quenching and static quenching. Among them, the dynamic quenching process corresponds to the Stern-Volmer equation. To determine the fluorescence quenching mechanism of RT, RT-Co(II) and RT-Ni(II) on BLF, the above systems were first treated according to the Stern-Volmer equation [24].

$$F_0/F=1+K_q\tau_0[Q]=1+K_{SV}[Q] \quad (2)$$

where F_0 and F are the fluorescence intensities in the absence and presence of quencher, respectively; K_q is the quenching rate constant of the biomolecule; τ_0 is the average fluorescence lifetime of the biomolecule without RT/RT-M^{2+}; [Q] is the concentration of the quenchers, mol·L^{-1}; K_{sv} is the Stern-Volmer quenching constant, L·mol^{-1}(K_q=K_{sv}/τ_0).

From Fig 7 and Table 3, we can see that in a wide range of concentrations of RT/RT-M^{2+}, the Stern-Volmer plots of BLF showed a good linear trend. It is well-known that the maximum scatter quenching constant K_q of various quenchers with biomacromolecules is 2.0×10^{10} L·mol^{-1}·s^{-1}. Obviously, the constant rate of BLF quenching procedure initiated by RT/RT-M^{2+} was greater than that of the scatter procedure, indicating that RT/RT-M^{2+}-BLF systems are static quenching, which means that the interaction mechanism between BLF and RT/RT-M^{2+} was not initiated by dynamic collision but from the formation of a stable complex.

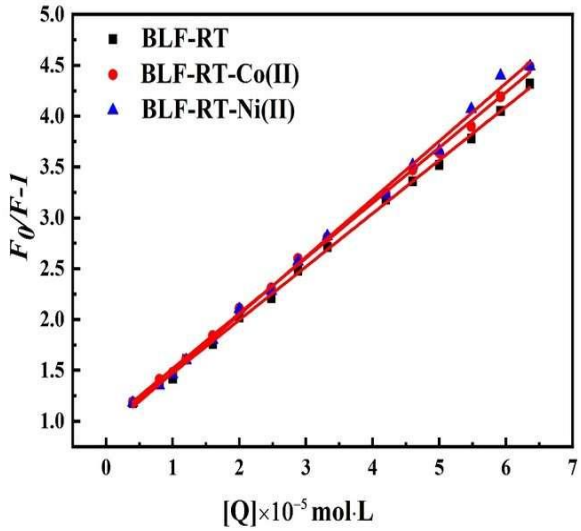

Fig. 7: Stern-Volmer plot of RT/RT-Co (II) /RT-Ni (II) binding with BLF. (RT/RT-Co (II) /RT-Ni (II) (×10-5mol·L-1): 0.40, 0.80, 1.00, 1.20, 1.60, 2.04, 2.48, 2.88, 3.32, 4.20, 4.60, 5.04, 5.48, 5.92, 6.36).

The Stern-Volmer quenching constant K_{sv} and the quenching rate constant K_q of BLF-RT, BLF-Co (II) -RT and BLF-Ni (II) -RT solution systems were calculated by Stern-Volmer equation and the results are shown in Table-3.

Table-3: The quenching constants of RT, RT-Co (II) and RT- Ni (II) to BLF.

Solution system	K_{sv} (10^4L·mol^{-1})	K_q (L·mol^{-1}·s^{-1})	R^2 (correlation coefficient)
BLF-RT	5.2	5.2×10^{12}	0.9989
BLF-Co (II) -RT	5.7	5.7×10^{12}	0.9988
BLF-Ni (II) -RT	5.4	5.4×10^{12}	0.9976

The binding parameters of RT, RT Co (II) and RT Ni (II) with BLF

The binding interaction parameters drugs and proteins can be evaluated by Scatchard model

$$v = nK[D]/(1+K[D]) \quad (3)$$

Here, v is the average number of drug molecules bound per protein molecule, n is the number of binding sites, K is the intrinsic binding constant, L·mol^{-1}, and [D] is the concentration of free drug, mol·L^{-1}. For the selected emission wavelength, if the fluorescence of the system is generated only by proteins, there are.

$$F/F_0=[P_t]/[P] \quad (4)$$

According to the definition of v, another equation is also known,

$$v=([D_t]-[D])/[P_t]=n([P_t]-[P])/[P_t]=n(F_0-F)/F_0=n\Delta F/F_0 \quad (5)$$

where [D_t] is the final concentration of drug and [P_t] is the total protein concentration; F_0 and F are, respectively, the fluorescence intensity in the absence of a quencher and in its presence at [D] concentration, $\Delta F= F_0 - F$.

From equation (3) and equation (4), we can deduce equation (5).

$$2\Delta F / F_0 = 1+1/Kn[P_t]+[D_t]/n[P_t]- \sqrt{(1+1/Kn[P_t]+[D_t]/n[P_t])^2-4[D_t]/n[P_t]} \quad (6)$$

The binding parameters of the binding reaction system can be obtained by non-linear fitting using equation (5). According to equation (5), the obtained experimental data are converted into 2 $\Delta F/F_0$, fitted to the experimental data of [Dt]/[Pt] to obtain a fitting curve (Fig 8), and then the binding constant K and the number of binding sites n of RT, RT Co(II) and RT Ni(II) are calculated by BLF. The results are given in Table 4.

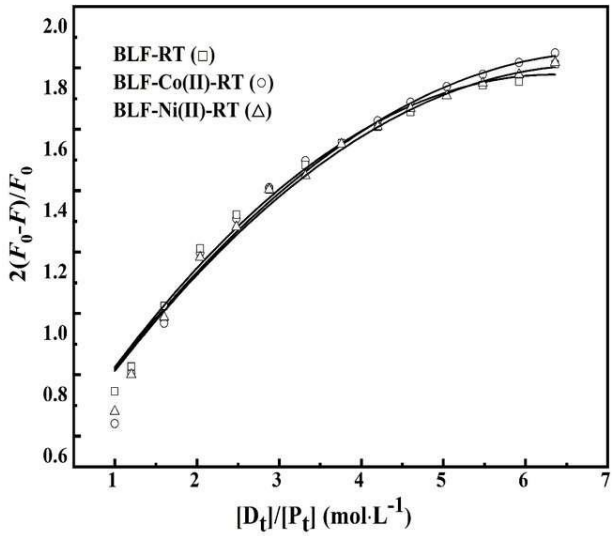

Fig 8: Non-linear fitting curve for the interaction of RT/RT-Co (II) /RT-Ni (II) binding with BLF.

In addition, to compare the differences and similarities in the calculation results of binding reaction parameters between different theoretical models, the Lineweaver-Burk double reciprocal equation was also used to fit the binding constant in this article:

$$(F_0\text{-}F)^{-1} = F_0 + K^{-1}F_0^{-1}[D]^{-1} \quad (7)$$

where F_0 and F are the fluorescence intensities in the absence and presence of the quencher, respectively; [D] is the concentration of the quencher (drug), mol·L^{-1}; K is the binding constant, L·mol^{-1}. The binding constants of RT/RT-M^{2+} and BLF were calculated from the slope and intercept of the Lineweaver-Burk plots as shown in Fig 9 (K=intercept/slope). The results are also shown in Table-4.

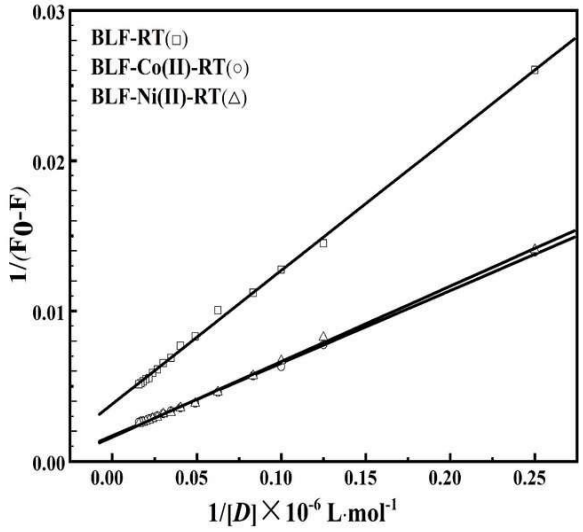

Fig. 9: Lineweaver-Burk plot for the interaction of RT/RT-Co (II) /RT-Ni (II) binding with BLF. Conditions: pH =7.40, λ_{ex}=282*nm*,$c_{BSA/BLF}$=1.0×10^{-5} mol·L$^{-1.}$

Table-4: The binding parameters of RT, RT-Co (II) and RT-Ni (II) to BLF.

Solution system	K②(L·mol^{-1})	K②(L·mol^{-1})	n①	R①	R②
BLF-RT	7.02×10^4	2.92×10^4	4.12	0.9750	0.9988
BLF-Co (II) -RT	7.37×10^4	3.54×10^4	4.18	0.9877	0.9992
BLF-Ni (II) -RT	7.15×10^4	3.24×10^4	3.88	0.9831	0.9990

①calculated by equation (5); ② calculated by equation (6)

From Figs 8 and 9 combined with Table 4, it can be seen that the results obtained from formulae (5) and (6) have good correlation coefficients and high order of binding constants, indicating that RT molecules, RT Co(II) molecules and RT Ni(II) molecules all form stable complexes with BLF. This also indirectly confirms that the mechanism of endogenous fluorescence quenching in BLF is static quenching. Meanwhile, by analysing the experimental results, the following rules were obtained: (1) Under metal ion mediation, the binding constant between RT and BLF is larger than that without mediation, and metal ion mediation makes the binding between RT and BLF closer and more stable; (2) The degree of influence of different metal ions on the binding reaction of BLF-RT varies, and the order of binding constants is $K_{\text{BLF-Co (II) -RT}} > K_{\text{BLF Ni (II)-RT}} > K_{\text{BLF-RT.}}$

From this, we boldly speculate that the influence of Co (II) and Ni (II) on the interaction site between turmeric glycosides and BLF molecules is a complex result of the combined action of non-covalent bridging and covalent interactions. In this work, the site binding model and the Lineweaver-Burk double reciprocal equation were used to process the spectral data of the binding reaction, and basically consistent results were obtained, demonstrating the credibility of the results analysis and further verifying the conclusion that metal ion mediation may play a complex role in the RT-BLF binding reaction.

The binding distance between RT, RT Co (II) and RT Ni (II) and BLF

The energy transfer efficiency between protein and RT can be calculated based on the non-radioactive energy of Förster [26], and the distance between the receptor and donor can be calculated using the transfer theory [26]. The internal filter effect has been corrected. The energy transfer efficiency E can be achieved by combining the distance r and the critical energy transfer distance R_0.

$$E = R_0^6/(R_0^6 + r^6) \quad (8)$$

Here, E is the transfer efficiency and R_0 is the critical distance when the transfer efficiency is 50%.

$$R_0^6 = 8.8\times10^{-25}K^2N^{-4}\Phi J \quad (9)$$

where, K^2 is the spatial orientation factor between the emission dipole of the donor and the absorption dipole of the acceptor; N is the refractive index of the medium; Φ is the fluorescence quantum yield of the donor, and J is the overlap integral of the fluorescence emission spectrum of the donor and the absorption spectrum of the acceptor. J can be described as [27]:

$$J = \int_0^\infty F(\lambda)\varepsilon(\lambda)\lambda^4 d\lambda \Big/ \int_0^\infty F(\lambda)d\lambda \quad (10)$$

where, F (λ) is the fluorescence intensity of the fluorescence donor at wavelength λ and ε (λ) is the molar absorptivity of the acceptor at wavelength λ, L·mol^{-1}·cm^{-1}.

The energy transfer efficiency E can be calculated by equation (10) [28]:

E=1-F/F_0 (11)

Thus, the overlap of the absorption spectrum of RT/ RT-Co (II) /RT-Ni (II) and the fluorescence emission spectrum of BLF is shown in Fig 10.

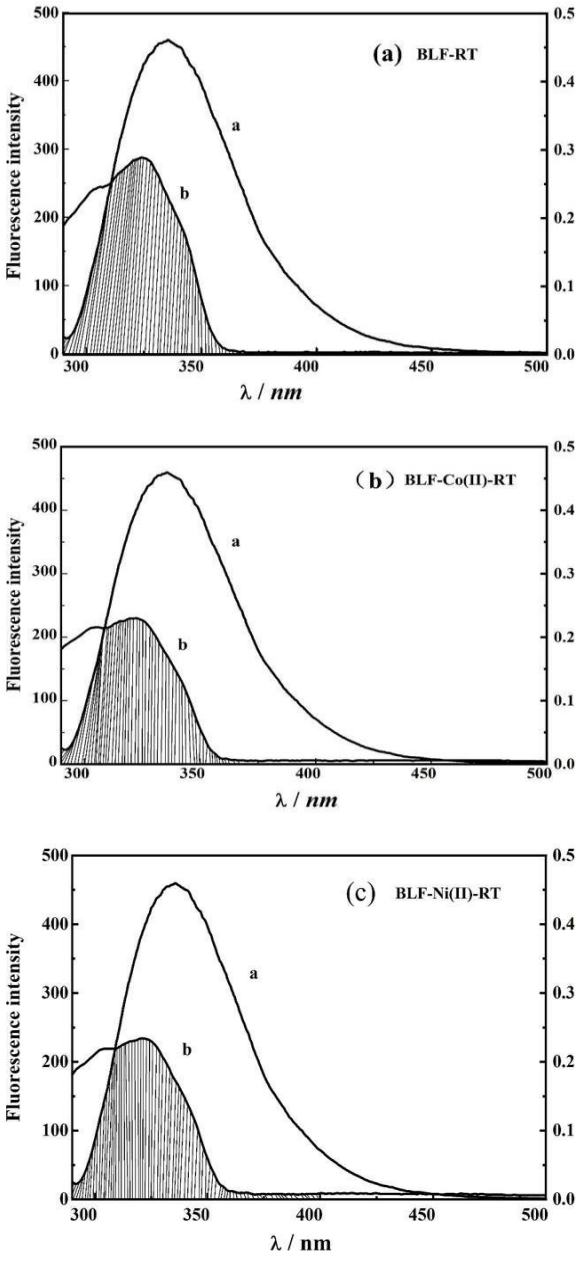

Fig. 10: Overlap of the fluorescence emission spectrum of BLF(a) with the absorption spectrum of RT (a)/RT-Co (II) (b)/RT-Ni (II) (c) [b]. (a: BLF-RT; b BLF-Co-RT; c: BLF-Ni-RT.).

Calculate the spectral overlap integral JBLF-RT, J_{BLF} Co(II)-RT and Ni(II)-RT of the RT/RT-M^{2+}-BLF binding reaction from equation (9) based on experimental data. The results are given in Table 5.

Table-5: The energy transfer parameters between quenchers and BLF [(a)].

Solution system	J / (cm^3·L·mol^{-1})	R_0/ nm	E	r/nm
BLF-RT	1.82×10^{-14}	2.73	0.3474	3.03
BLF-Co(II)-RT	1.41×10^{-14}	2.64	0.3821	2.86
BLF-Ni(II)-RT	1.47×10^{-14}	2.69	0.3594	2.96

a)N=1.36，Φ=0.118，K^2=2/3.

From Table 5 we can see that the binding distances between RT/RT-Co (II) /RT-Ni (II) and BLF are all less than 7 nm, indicating that there is nonradioactive energy transfer between RT/RT-M^{2+} and BLF. The addition of Co (II) and Ni (II) has made the binding distance decreased by 0.17nm and 0.07nm, respectively, indicating that the addition of Co (II) and Ni (II) has made the BLF-RT complex more stable. This result is also consistent with the previous experimental result of binding parameters.

The effect of RT/RT-Co (II) /RT-Ni (II) on the microconformation of BLF

By fixing the protein concentration and gradually increasing the concentration of RT/RT Co(II)/RT Ni(II), the synchronous fluorescence scanning reaction system can obtain the synchronous fluorescence spectrum of BLF (Fig 11).

From Fig 11(A), it can be seen that the fluorescence of BLF is mainly contributed by tryptophan. As the concentration of RT/RT-M^{2+}increases, Δλ=The maximum emission wavelength of the synchronous fluorescence spectrum at 60 nm undergoes a red shift (about 16 nm), Δλ=The maximum emission wavelength of the synchronous fluorescence spectrum at 15 nm remains basically unchanged, indicating that the addition of RT, RT Co (II), and RT Ni (II) under the experimental conditions has a certain effect on the conformation of the micro-regions around the tryptophan residues in the BLF molecule, increasing the extension of the peptide chain and the relative expansion of the hydrophobic cavity of the micro-regions, exposing some tryptophan residues to the polar solvent environment to a greater extent, resulting in a decrease in the hydrophobicity of the surrounding region [29].

Meanwhile, from the synchronous fluorescence spectrum of BLF-M^{2+} in the upper right corner of Fig 11(B/C), it can also be seen that metal ions Co (II) and Ni (II) have weak fluorescence quenching effects on the tryptophan and tyrosine

residues of BLF molecules; however, the synchronous fluorescence quenching effect of the reaction system is mainly due to the quenching of the fluorescence of RT molecules with BLF tryptophan and tyrosine residues. The maximum fluorescence emission peak positions of metal ions Co (II) and Ni (II) on the interaction of tryptophan and tyrosine residues in BLF molecules have not changed, indicating that Co (II) and Ni (II) alone do not change the conformation of BLF molecules in solution.

BLF is composed of 689 amino acids, with 13 tryptophan residues in the molecule. Its three-dimensional structure forms two circular structures at the N and C ends of the molecule [30], respectively. Although the research on the binding sites between BLF and drug molecules is not completely clear, by analyzing the three-dimensional structure of BLF and the position of tryptophan on BLF macromolecules, and combining with literature reports, we further analyze the experimental data on the interaction between RT/RT-M^{2+}molecules and BLF in this experiment. We speculate that RT molecules are likely to bind near Trp 125 residues or Trp 467 residues with relatively high binding activity due to hydrophobic interactions, the conformational changes in the surrounding microregions result in an increase in the extension of the peptide chain, resulting in a decrease in the hydrophobicity of the surrounding area.

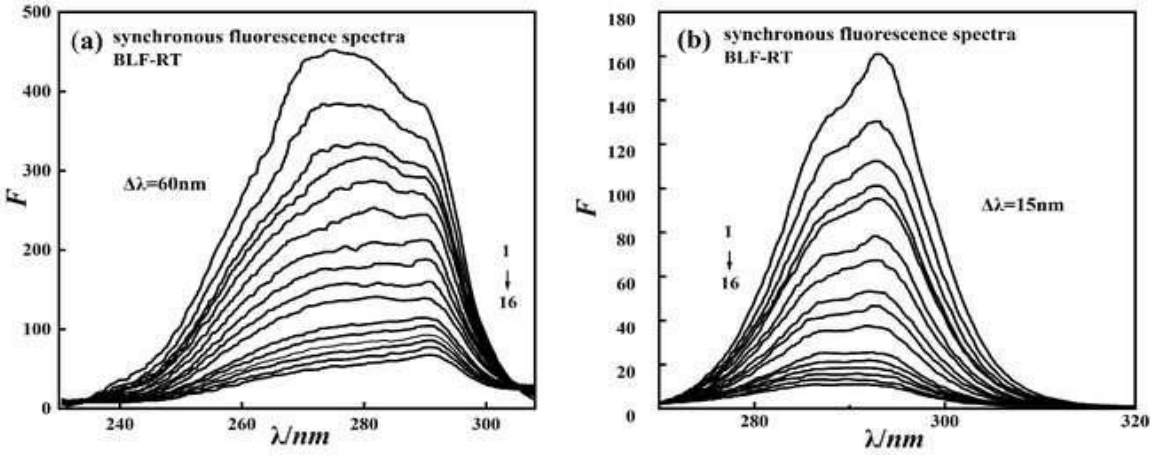

Fig. 11: (A) : Effect of RT on the synchronous fluorescence spectra of BLF.

(a: $\Delta\lambda$=60*nm*, b: $\Delta\lambda$=15*nm*; c_{BLF}=1.0×10^{-5}mol·L^{-1}; c_{RT} (×10^{-5}mol·L^{-1}), 1 to 16: 0, 0.40, 0.80, 1.00, 1.20, 1.60, 2.04, 2.48, 2.88, 3.32, 4.20, 4.60, 5.04, 5.48, 5.92, 6.36.)

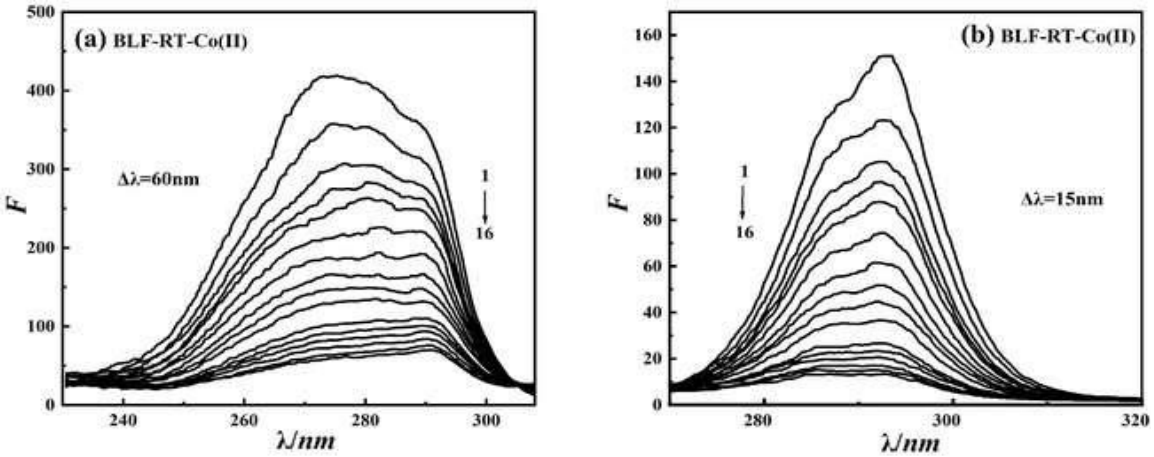

Fig. 11: (B) : Effect of RT-Co (II) on the synchronous fluorescence spectra of BLF.
[The up diagram is the synchronous fluorescence spectra of BLF in the presence of Co (II)].

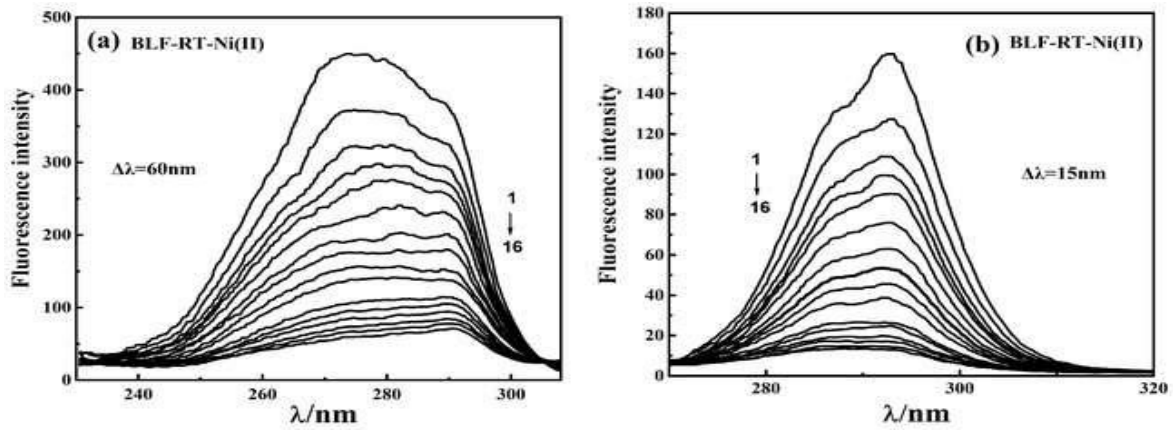

Fig. 11: (C) : Effect of RT-Ni(II) on the synchronous fluorescence spectra of BLF.

(a: $\Delta\lambda$=60*nm*, b: $\Delta\lambda$=15*nm*; c_{BLF}=1.0×10^{-5}mol·L^{-1}; $c_{RT\text{-}Ni(II)}$ (×10^{-5}mol·L^{-1}), 1 to 16: 0, 0.40, 0.80, 1.00, 1.20, 1.60, 2.04, 2.48, 2.88, 3.32, 4.20, 4.60, 5.04, 5.48, 5.92, 6.36.). [The up diagram is the synchronous fluorescence spectra of BLF in the presence of Ni (II) .]

Characterization the effect of RT/RT-Co (II) /RT-Ni (II) on the micro conformation of BLF

To precisely quantify the hydrophobicity and microconformation changes of BLF, we suggest using a new formula combining the above-mentioned two indices to describe the microconformation change of protein. E_D stands for "extension degree" of the microconformation of protein with the equation as follows:

$$E_D = (1 - F/F_0)\,\Delta\lambda \qquad (12)$$

where, F_0 and F are the fluorescence intensities in the absence and presence of quenchers, respectively. $\Delta\lambda$ is the maximum emission wavelength shift (we define red shift as positive value and blue shift as negative value) obtained from synchronous fluorescence spectra with $\Delta\lambda$=60 *nm*. The effect of RT, RT-Co (II) and RT-Ni (II) acting on the microconformation change of BLF's subdomain can be evaluated by plotting E_D vs. [*D*] in Fig 12.

From Fig 12 we can see that the difference of E_D value between the BLF-RT and BLF-M^{2+}-RT (M^{2+}=Co^{2+}, Ni^{2+}) solution systems are insignificant although they have a different E_D value. It is apparent that RT, RT-Co (II) and RT-Ni (II) have the approximate effect on microconformation of BLF. Physical studies show that a substantial conformational change of lactoferrin accompanies iron binding and release. Although this experiment can't reach the effect that the binding site of Co and Ni is different from the Fe binding site, however, this experimental data provides information on conformational change of lactoferrin being difference from Fe binding, Co (II) and Ni (II) can't affect the microconformation of BLF. As the concentration of quenchers increasing, the microenvironment around tryptophan residues in BLF becomes more exposed to the polar environment [31].

It can also be seen from the Fig 12 that the concentration effect of M^{2+} (M^{2+}=Co^{2+}, Ni^{2+}) on BLF's microconformation can be identified in this work, it should be considered as an influence factor for the interaction study. BLF-RT, BLF-Co (II) -RT and BLF-Ni (II) -RT solution systems nearly have the same effect on BLF's microconformation when quenchers concentration is less than 4.5×10^{-5}mol·L^{-1}, but with the quenchers concentration over 5×10^{-5} mol·L^{-1}, the extension degree of the microconformation around tryptophan residues in BLF increases dramatically in the beginning, and then increasing slightly with more quenchers were titrated into BLF solution. Along with the concentration of RT/RT-M^{2+} increasing, the extension degree of the microconformation around tryptophan residues in BLF almost meet the saturation level, the changes of E_D are not at all evident. It can be obtained from the result that the E_D can quantitatively measure the transformation degree of the peptide chain in process of drug molecule acting on protein molecule, E_D can intuitively mirror the influence of drug on microconformation of protein.

Effect of RT, RT-Co (II) and RT-Ni (II) on the binding sites of BLF

In order to directly visualize the effect of RT/RT-Co (II) /RT- Ni (II) on the synchronous

fluorescence spectra of BLF to evaluate the interaction extent between RT/RT-M^{2+} and tryptophan and tyrosine residues (binding sites) of BLF molecule. The binding trend curve by plotting F/F0 against [D]/[P] ([D]/[P] is the concentration ratio of RT/RT-M^{2+} and BLF) was made, Fig 13 is obtained according to the experimental data of the synchronous fluorescence spectra.

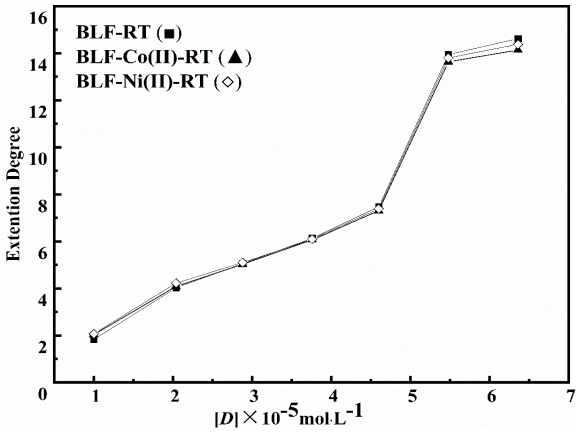

Fig. 12: The relationship between extension degree and the concentration of RT/RT-M (II).

From Fig 13, it can be seen that when [*D*]/[*P*] is small, which means the concentration of the drug is small, the trend of the binding sites of BLF influenced by RT/RT-Co (II) /RT-Ni (II) is consistent with the result of binding constant. The mediated effect of Co (II) and Ni (II) is noticeable in the binding interaction between RT and BLF when the [*D*]/[*P*] values is only within low, and the situation is at the opposite when the concentration of drug is increasing. It can be attributed to the strong binding sites of BLF having been occupied with increasing the drug molecule, and Co (II) and Ni (II) play the mediation effect in the process of RT interaction with BLF's strong binding sites.

Molecular docking and dynamic simulation analysis of the interaction between RT and BLF

Molecular docking analysis of intermolecular interactions between RT and BLF

The method of using RT molecules to dock with BLF active sites to determine intermolecular interactions also further validates the spectral experiments. The docking results are shown in Fig 14.

The binding site connecting RT and BLF is situated in the middle of the BLF molecule. Where necessary, technical terms will be explained upon first use. The Tyr319 fluorescence factor residues primarily form the binding sites for RT and BLF, elucidating the mechanism behind BLF fluorescence quenching. In the diagram, the amino acids for RT are Leu308, Arg689, Gly321, Leu318, Leu385, Lys386, Leu687, Cys405, Leu407, Gly406, Arg600, Asp602, Ser601, Arg323, Ser322, Leu320, Thr90, His91, Tyr319, Pro251, Ser252, Phe686. Of these, Thr90, Gly406, and Cys405 form hydrogen bonds, which increase the affinity and stability between the two. This has implications for the absorption, metabolism, and dose response of RT in organisms. Phe686 features weak π-π stacking interactions between aromatic rings, which are equally significant for non-covalent interactions, including hydrogen bonds. Hydrophobic π-alkyl groups are formed by Tyr319 and Leu687. In addition, a chemical bond exists between carbon and hydrogen atoms, along with van der Waals forces. It is clear that hydrogen bonding and hydrophobic forces play a key role in the intermolecular interactions between RT and BLF.

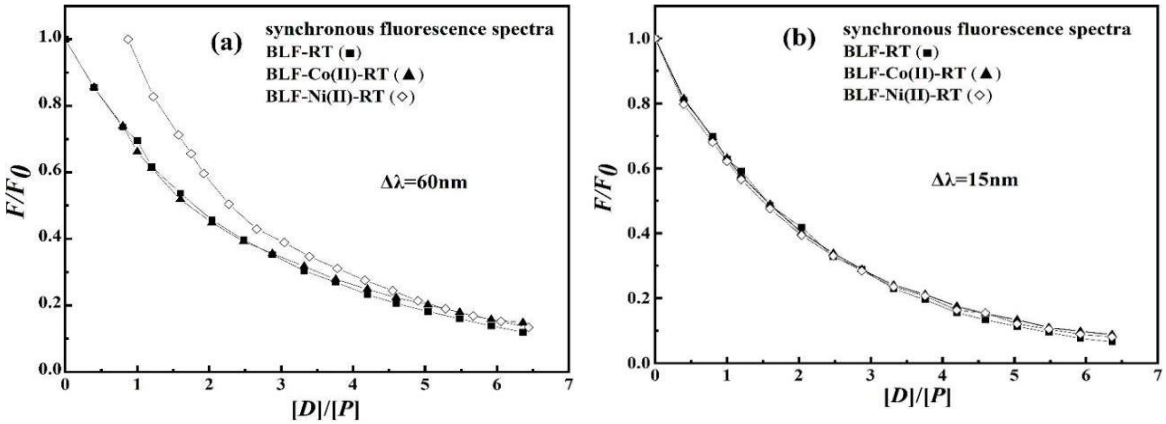

Fig. 13: The binding trend curve of BLF in the presence of various concentration of RT, RT-Co (II) and RT-Ni (II) Condition: c_{BLF}= 1.0×10^{-5} mol·L^{-1}.

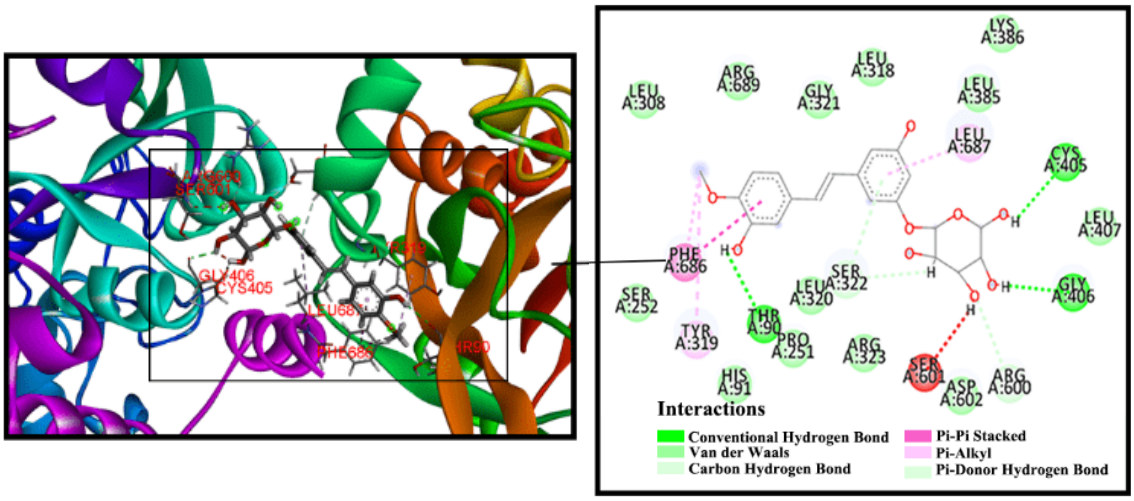

Fig. 14: Visualization results of molecular docking of RT and BLF.

Molecular dynamics simulation analysis of intermolecular interactions between RT and BLF

The molecular dynamics simulation is used to study the spatial conformation of the interaction between BIF and RT, with various parameters calculated in vitro. Fig 15 (a) illustrates that the root mean square deviation (RMSD) of BLF-RT is 2.18, whereas that of BLF is 2.09. The RMSD value is augmented by the addition of small molecules, which suggests augmented flexibility and the range of movement. In addition, the incorporation of small molecules causes alterations in the spatial configuration of proteins. Graph α illustrates that the backbone of the BLF single molecule system, as depicted in the Fig 15, displays an initial increase in the RMSD carbon value over the course of the dynamic simulation process. This may be attributed to the optimization of the molecules' internal structure. Nevertheless, the subsequent stabilization after 20 ns serves as evidence that the system has largely attained a state of equilibrium.

Fig 15 (B) indicates a decrease in the RMSF value following BLF-RT binding, suggesting an interaction between BLF amino acid residues and RT. Moreover, the RMSD of the active amino acids exhibits almost complete overlap and stability. The RMSF values of amino acids neighbouring the active site in BIF and BIF-RT are essentially similar and remain stable with minor variations. The adaptability of the region is deemed relatively low, indicating an increased vulnerability to perturbation by small molecules.

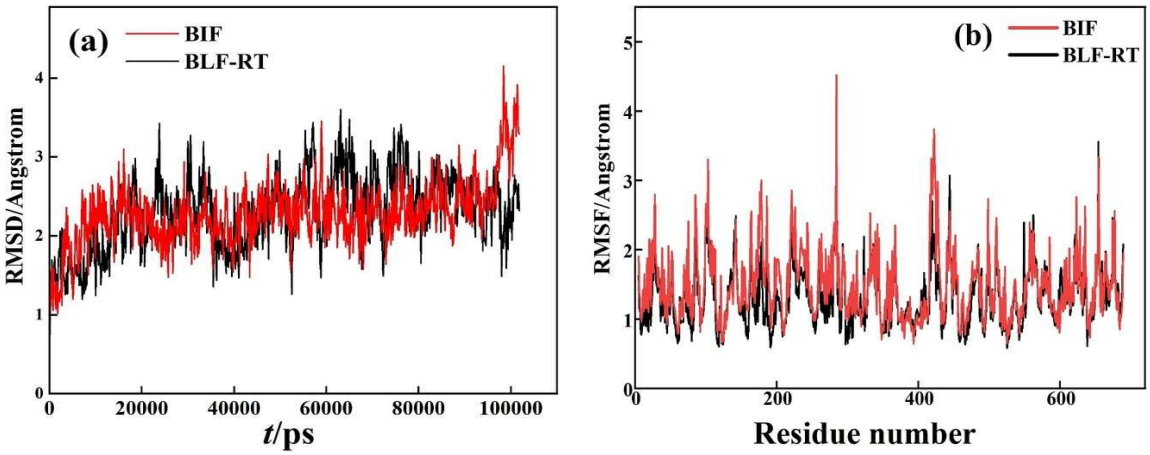

Fig. 15: Root mean square deviation RMSD and root mean square fluctuation RMSF curve.

(a) The curve of the RMSD value of BLF and RT-BLF over time;

(b) The RMSF value and time curve of the skeleton Co carbon atoms of BLF and RT-BLF systems

Conclusion

In this study, network pharmacology research methods were utilised to build network topology and biological information networks using high-throughput technology. The mechanism of how RT regulates cancer diseases associated with BLF may be linked to signal pathways, including P13-Akt, MAPK, and PD-LI. The molecular docking revealed that the binding energy of RT and BLF associated cancer core targets is similar to that of BLF. It is speculated that the binding effect of RT and BLF may reflect the strength of RT binding to associated cancer target proteins. This could demonstrate the pharmacological basis of RT on BLF-associated cancer target proteins. Using BLF as template and multispectral technology, an static complex between RT and BLF was confirmed. Additionally, Co (II) and Ni (II) mediation reduced the binding distance of BLF-RT by 0.22 nm and 0.14 nm, respectively. Technical abbreviations are explained upon their first appearance in the text. This suggests that the introduction of Co (II) and Ni (II) enhances the binding strength and stability of BLF-RT, which improved energy transfer efficacy promoting the interaction between RT and BLF. Molecular dynamics simulation and docking analyses confirm that RT alters the spatial configuration of BLF, with hydrogen bonding and hydrophobic interaction being the dominant binding forces between the two. The existence of hydrogen bonding reinforces the notion that BLF and RT form a securely bound composite.

This paper explains the molecular mechanism of rhodopsin (RT) and BLF-associated cancer diseases using network pharmacological analysis, which provides a basis for the next step in developing the research value of RT.Meanwhile, the interaction between RT and BLF provides an innovative strategy of "natural drugs-functional proteins-metal ions" for the treatment of cancer, which provides crtain theoretical support for the mechanism of BLF-related cancer diseases and certain theoretical reference for the treatment of BLF-related cancers.

Acknowledgments

This work was financially supported by the "Three Rural Nine Parties" science and technology collaboration project of Zhejiang province in China (NO. 2024SNJF038).

References

1. Y. C. Gu, J. P. Wu, Bovine lactoferrin-derived ACE inhibitory tripeptide LRP also shows antioxidative and anti-inflammatory activities in endothelial cells, *J. Funct. Foods*, **25**, 375-384 (2016).
2. J. H. Xu, T. L. Han, Z. Tang, Y. Yan and J. M. Li, Effects of theaflavins on the structure and function of bovine lactoferrin, *Food Chem.*, **338**, 120848 (2021).
3. L. Y. Hao, Q. Shan, J. Wei, F. T. Ma and F. Liu, Lactoferrin: major physiological functions and applications, *Curr. Protein Pept. SC.*, **20**, 139-144 (2019).
4. B. Wang, Y. P. Timilsena, E. Blanch and B. Adhikari, Lactoferrin: Structure, function, denaturation and digestion. *Cri. Rev. Food Sci*., **59**, 580-596 (2019).
5. X. Wang, Y. Liu and L. L. He, Spectroscopic investigation on the food components–drug interaction: The influence of flavonoids on the affinity of nifedipine to human serum albumin, *Food Chem. Toxicol*., **78**, 42-51 (2015).
6. J. Kim, Y. Ma, Rhaponticin decreases the metastatic and angiogenic abilities of cancer cells via suppression of the HIF-1α pathway, *J. Oncol*., **53**, 1160-1170 (2018).
7. R. G. Li and A. Chinnathambi, Anti-inflammatory effects of rhaponticin on LPS-induced human endothelial cells through inhibition of MAPK/NF-κβ signaling pathways, *J. Biochem. Mol. Toxic*., **35**, e22733 (2021).
8. R. Zhang, K. A. Kang and M. J. Piao, Rhapontigenin from Rheum undulatum protects against oxidative-stress induced cell damage through antioxidant activity, *J. Toxico*l. *Environ. Health*, **70**, 1155-1166 (2007).
9. K. Banik, A. M. Ranaware, N. Thakur, S. Girisa, V. Despande and L. Fan, Piceatannol: A natural stilbene for the prevention and treatment of cancer, *Pharmacol. Res*., **153**, 104635 (2016).
10. A, Xin Qi , *et al*. Studying the interaction mechanism between bovine serum albumin and lutein dipalmitate: Multi-spectroscopic and molecular docking techniques - ScienceDirect. Food Hydrocolloids (2020).
11. S. L. Zhuang, H. F. Wang and K. K. Ding, Interactions of benzotriazole UV stabilizers with human serum albumin: atomic insights revealed by biosensors, spectroscopies and molecular dynamics simulations, *Chem*., **144**, 1050-1059 (2016).
12. Chen M, Zhu J, Kang J, Lai X, Gao Y, Gan H, Yang F. Exploration in the Mechanism of Action of Licorice by Network Pharmacology. Molecules. 2019; 24(16):2959.
13. B, Moamen S. Refat A , *et al*. Synthesis, spectroscopic, thermal and antimicrobial

investigations of new mono and binuclear Cu(II), Co(II), Ni(II), and Zn(II) thiosemicarbazide complexes - ScienceDirect. Journal of Molecular Structure 1218(2020).
14. Tian, Luwei Tian Luwei , M. G. M. Guo , and X. L. Shi. Imaging Serum Proteome Behavior in Process of Lead Transportation in Vivo: A Fluorescence Spectroscopic Analysis Insight. Journal of the chemical society of pakistan (2022).
15. J. L. Ru, P. Li and J. N. Wang, TCMSP: a database of Systems pharmacology uncovers Janus functions of botanical drugs: activation of host defense system and inhibition of influenza virus replication, *Inte*. *Biol*., **5**, 351-371 (2013).
16. [X. Wang, Y. H. Shen and S. W. Wang, Pharm Mapper 2017 update: a web server for potential drug target identification with a comprehensive target pharmacophore database, *Nucleic*. *Acid Res*., **45**, 356-360 (2017).
17. L. Ren, L. J. Wang and Y. Zong, Study on the mechanism of quercetin in the treatment of type 2 diabetes based on network pharmacology and molecular docking, *J. Drug Eval*. *Res*., **43**, 1964 (2020).
18. E Coudert, S Gehant, E de Castro, M Pozzato, D Baratin, T Neto, C J A Sigrist, Nicole Redaschi, A Bridge, The UniProt Consortium , Annotation of biologically relevant ligands in UniProtKB using ChEBI, Bioinformatics, Volume 39, Issue 1, January 2023, btac793.
19. D Szklarczyk, R Kirsch, M Koutrouli, K Nastou, F Mehryary, R Hachilif, A L Gable, T Fang, N T Doncheva, S Pyysalo, P Bork, L J Jensen, C von Mering, The STRING database in 2023: protein–protein association networks and functional enrichment analyses for any sequenced genome of interest, Nucleic Acids Research, Volume 51, Issue D1, 6 January 2023, Pages D638–D646.
20. W. C. Dan, Q. Y. HE, Y. Qu and A. Q. Li, Molecular mechanism of Zhizhu pills in regulating dyslipidemia based on network pharmacology, *J. World Sci. Technol. Mod. Tradit. Chin. Med. Mater. Med*., **21**, 2396-2409 (2019).
21. Y. Y. Zhou, B. Zhou, Metascape provides a biologist-oriented resource for the analysis of systems-level datasets, *Nat*. *Commun*., **10**, 1038-1048 (2019).
22. H. M. Berman, K. Henrick and H. Nakamura, Announcing the worldwide Protein Data Bank, *Nat*. *Struct*. *Mol. Biol*., **10**, 980-980(2003).
23. K. Osama and I. K. Al-Shihi, Characterization of subdomain IIA binding site of human serum albumin in its native, unfolded, and refolded states using small molecular probes, *J*. *Am*. *Chem*. *Soc.*, **130**, 10793-10801 (2008).
24. X. Y. Ran and X. W. Lu, Interaction of Cr (VI) binding with bovine serum albumin: reaction mechanisms and thermodynamic properties, *Asian J*. *Chem*., **25**, 4689-4692 (2013).
25. Fathy, Mona E. , Mohamed I. El-Awady, and F. Belal. "Simultaneous determination of metolazone and losartan in their combined tablets using synchronous fluorescence spectroscopy." Luminescence 34(2019).
26. M. Guo, X. W. Lu and Y. Wang, Comparison of the interaction between lactoferrin and isomeric drugs, *Spectro. Chim*. *Acta*., **173**, 593-607 (2017).
27. R. Elaheh, M. Mahmoodian-Moghaddam, S. Khorsand-Ahmadi and J. Chamani, Binding site identification of metformin to human serum albumin and glycated human serum albumin by spectroscopic and molecular modeling techniques: a comparison study, *J. Biomol. Struct. Dyn.,* **33**, 513-533 (2015).
28. H. J. Liu, Y. Dong, J. Wu, C. D. Chen, D. D. Liu and Q. Zhang, Evaluation of interaction between imidazolium-based chloride ionic liquids and calf thymus DNA, *Sci*. *Total Environ*., **566**, 1-7(2016).
29. Ma, Gamaliel Junren , *et al*. "Conformational flexibility of fatty acid-free bovine serum albumin proteins enables superior antifouling coatings." Communications Materials 1.1(2020).
30. H. Aghabozorg, J. Attar. Gharamaleki and M. Ghadermazi, Piperazinium hexaaquacobalt (II) bis[bis(pyridine-2,6-dicarboxylato) cobaltate (II)] octa-nydrate, *Acta Cryst*., **63**, 1803-1804 (2007).
31. M. Guo, X. M. Wang and Y. T. Zuo, Comparative analysis of the interaction of HSA and BSA with tyrosine kinase inhibitorimatinib by spectroscopic and molecular simulation, *Chin*. *J*. *Biochem*. *Mol*. *Biol.*, **31**, 723-733 (2015).